This is a preprint, the final version is subject to change, of the American Mineralogist (MSA)
Cite as Authors (Year) Title. American Mineralogist, in press.
(DOI will not work until issue is live.) DOI: http://dx.doi.org/10.2138/am-2016-5436

Revision 3

Discovery of *in situ* super-reducing, ultrahigh-pressure phases in the Luobusa ophiolitic chromitites, Tibet: New insights into the deep upper mantle and mantle transition zone *

RU Y. ZHANG[1,2,3*], JING-SUI YANG[1], W. G. ERNST[3], BOR-MING JAHN[2], YOSHIYUKI IIZUKA[4], AND GUO-LIN GUO[1]

[1] *CARMA, State Key Laboratory of Continental Tectonics and Dynamics, Institute of Geology, Chinese Academy of Geological Sciences, Beijing, 100037, China*

[2] *Dept. of Geosciences, National Taiwan University, Taipei 106, Taiwan, ROC*

[3] *Dept. of Geological Science, Stanford University, Stanford, CA 94305-2155, USA*

[4] *Institute of Earth Sciences, Academia Sinica, Taipei, Taiwan, 11529, ROC*

ABSTRACT

Previous research on super-reducing ultrahigh-pressure (SuR UHP) phases from the Tibetan ophiolitic chromitites were mainly conducted on isolated grains extracted from extremely large samples. This approach has been questioned because of possible contamination. To elucidate the occurrence and origin of these SuR UHP minerals, we studied 33 thin sections and rock chips of three ophiolitic chromitites from the Yarlung

* E-mail: ruyzhangpan@yahoo.com

Zangbo suture zone**.** Here we report and analyze unambiguously *in situ* SuR UHP assemblages from the ophiolitic chromitites by electron probe micro-analyzer, scanning microscope and Laser Raman spectroscope. The SuR UHP and associated phases include: (1) blue moissanite as inclusions in olivine (Fo_{96-98}), and in olivine domains between disseminated chromite grains; (2) multiple inclusions of moissanite + wüstite + native Fe in olivine; (3) FeNi and FeCr alloys in olivine and chromite; and (4) native Fe and Si in chromite. Crustal asphaltum and h-BN also occur as inclusions in chromite. Our documented *in situ* SuR UHP phases, combined with the previously inferred existence of ringwoodite + stishovite, all indicate that these assemblages formed under a highly reducing environment (oxygen fugacities several orders of magnitude lower than that of the iron-wüstite buffer) in the mantle transition zone (MTZ) and in the deep upper mantle. Diamond + moissanite with distinct ^{13}C-depleted compositions from chromitites have a metasedimentary carbon source. Associations with existing crustal minerals in chromitites demonstrate that carbon-bearing metasedimentary rocks were recycled into the mantle through subduction, and locally modified its composition. Finally we propose a 3-stage model to explain the formation of SuR UHP phase-bearing chromitite. Discoveries of SuR UHP phases in Luobusa and other ophiolitic podiform chromitites from the polar Ural Mountains and from Myanmar imply existence of a new type of ophiolitic chromitite. Such occurrences provide an additional window to explore the physical-chemical conditions of the MTZ, mantle dynamics, and the profound recycling of crustal materials.

Keywords: ophiolitic chromitite, *in situ*, super-reducing UHP phases, deep upper mantle, mantle transition zone, Tibet, moissanite, wüstite

INTRODUCTION

Ophiolites are traditionally considered as the remnants of ancient oceanic crust and upper mantle that formed in low-pressure rift settings, and subsequently were emplaced onto active continental margins (Dilek and Furnes 2014). Podiform chromitites spatially associated with ophiolites are thought to have formed at shallow depths by mantle melt or rock - melt reactions (e.g., Coleman 1977; Zhou et al. 1996). However, documented occurrences of diamonds and other UHP minerals in ophiolitic podiform chromitites and associated peridotites along the Yarlung Zangbo suture zone, Tibet, as well as in the Polar Urals, and in Myanmar (Yang et al. 2014, 2015) suggest a deep-seated stage in the formation of ophiolitic podiform chromitites.

The Luobusa ophiolite crops out along the eastern segment of the Yarlung Zangbo suture between the Indian plate and the Lhasa block (Fig. 1a); it is a fault-bounded slab lying between Tertiary molasse deposits of the Luobusa Formation and the Gangdese batholith to the north, and Triassic flysch deposits to the south (Robinson et al. 2004) (Fig. 1b). The ophiolite evidently formed at a mid-ocean ridge (Zhou et al. 1996) at 162.9 ± 2.8 Ma, as indicated by U-Pb SHRIMP analyses of zircon from comagmatic diabase dikes (Zhong et al. 2006). Podiform chromitites within upper mantle harzburgites probably formed later by rock-melt reaction in a suprasubduction zone at ~126-120 Ma (Malpas et al. 2003; Yamamoto et al. 2013; Zhou et al. 2005, 2014). This ultramafic complex then sank to the mantle transition zone (MTZ), and later ascended to uppermost mantle depths by convection (Arai 2013).

Over the past 25 years, many unusual minerals have been separated and identified from large samples (500 to > 2000 kg) of the Luobusa podiform chromitite and its harzburgite wall rock (Bai et al. 1993, 2000, 2003; Robinson et al. 2004; Xu et al. 2009; Yang et al. 2014).

Minerals include: (1) quartz, feldspars, andalusite, almandine and zircon (Robinson et al. 2015; Xu et al. 2015; Yamamoto et al. 2013). Zircon xenocrysts (U-Pb age range: 100-2700 Ma) also contain low-*P* mineral inclusions such as feldspar, quartz, rutile, ilmenite, muscovite and andalusite; the zircon xenocrysts are chiefly older than the formation ages of both chromitite and ophiolite, and have a continental crust origin. Three younger ages of ~100 Ma probably result from Pb loss (Yamamoto et al. 2013). (2) SuR UHP minerals, especially diamond and moissanite. (3) Super-reducing native Fe, Ti, Si Mn, and a wide range of alloys (*e.g.*, Ni-Fe-Cr-C, Fe-Ni-Si, Cr-Fe, Ni-Mg-Co and W-Ta) are present in some chromite pods (see review by Liou et al. 2014 and appendix Table A1). Moreover, Robinson et al. (2004) inferred the former existence of ringwoodite (P>18 GPa) attached to a chromite grain, based on Mg-Fe silicates that display octahedral morphology and a spinel structure. Similarly, the presence of stishovite (P>9 GPa at 1000 ^{o}C) was inferred based on intergrowths of elongate coesite prisms and an unknown amorphous phase crosscut by later kyanite (Yang et al. 2007); these silicate aggregates decorate the rims of a rounded FeTi alloy bleb. Some chromite crystals contain coesite and clinopyroxene exsolution lamellae. The latter probably had a precursor possessing the $CaFeO_4$ (CF) structure and formed at 12.5 GPa (Yamamoto et al. 2009). Recent high *P-T* experiments on the $MgCr_2O_4$ transition indicated that the chromite formed at <12-15 GPa, based on absence of the assemblage $(Mg,Fe)_2Cr_2O_5$ + Cr_2O_3 (corundum-type) in Luobusa chromitites (Ishii et al. 2015). Thus, the coesite-bearing chromite undoubtedly formed under UHP conditions.

Our identification of SuR UHP assemblages in the Luobusa chromitites challenges traditional hypotheses about the origin of podiform chromitites associated with ophiolites, and raises provocative questions. What was the source region of the SuR UHP minerals? More

perplexing, how did these SuR UHP phases become associated with clearly crustal materials in the Luobusa chromitite? What was the origin of the SuR UHP mineral-bearing chromitites?

Except for the diamond inclusions (Yang et al. 2014) and coesite lamellae in chromite (Yamamoto et al. 2009) recently demonstrated to be *in situ*, all earlier research on UHP minerals and SuR UHP phases were conducted on grains separated from ophiolitic chromitites, not on *in situ* inclusions within the chromite and olivine themselves. Occurrences of separated minerals are enigmatic, because possible contamination of the separates is a major concern. In this study (1) we first document the unambiguous occurrence of inclusions of these SuR UHP and associated phases in chromite and olivine from the basal portion of the Luobusa chromitite and a few rare crustal minerals. (2) Then we discuss the inferred ultimate source regions of the SuR UHP and associated phases and their redox conditions. Formation and stabilization of the *in situ* SuR phases require oxygen fugacities below the iron-wüstite buffer in the deep upper mantle and the mantle transition zone. Studies of SuR UHP assemblage-bearing ophiolitic chromitites have thus opened a new window on the deep upper mantle and the mantle transition zone (MTZ), as well as documenting the profound recycling of crustal materials.

SAMPLE PREPARATION AND ANALYTICAL PROCEDURES

Nine polished thin sections and 24 discs of polished rock chips were made of 9 chromitite specimens from three ore deposits (Kanjinla, Xiangkashan and Luobusa; Fig. 1b) in the Luobusa area (hereafter termed the Luobusa ophiolitic chromitites). One thin section (YK15), and 2-4 discs of thin rock chips (YK15A, B, C, D) were made from each sample by conventional methods. For the discs of polished rock chips, the selected specimen was sliced (~1 mm thick) employing a micro-diamond saw. Cleaned samples were cold-mounted at room

113 temperature and cured for eight hours in epoxy resin (Epofix: Struers Co) with a 1-inch
114 diameter mold. Mounted samples were ground with silicon carbide (gray to colorless) papers
115 from #400 to #2000 (or P-4000), then polished with alumina compounds (particle size from
116 3μm and 1μm) on a rotation disk made of PVC (thermoplastic resins), not metal. The final 2-4
117 day polish was made employing a vibration polisher with 0.3μm alumina compounds. During
118 sample preparation, no native Fe, Si, FeO and BN compounds were used. Techniques for our
119 diamond search were similar to the procedure described above, but the selected specimen was
120 sliced ~1 cm thick.

121 First we investigated the thin sections and discs employing petrographic and binocular
122 microscopes, and marked suitable target areas. The micro-textures of target areas were studied
123 using a field emission scanning electron microscope (FE-SEM: JEOL JSM-7100F at the
124 Institute of Earth Sciences, Academia Sinica, Taipei); identifications of minerals were made by
125 an energy dispersive spectrometer (EDS: Oxford Instruments Ltd., INCA-350) equipped with
126 an FE-SEM, under beam conditions of 15 kV, and 0.1 nA acceleration voltage, and current,
127 respectively. The Raman spectra of moissanite, asphaltum and h-BN were determined by Laser
128 Raman spectroscope (RM1000) in the State Key Laboratory of Continental Tectonic and
129 Dynamics, Institute of Geology, Chinese Academy of Geological Sciences (CAGS). Spectral
130 resolution is 1 cm^{-1} and the excitation line of the laser is 514 nm. The compositions of olivine,
131 chromite, FeNi alloys and other phases were analyzed at the Institute of Earth Sciences,
132 Taiwan using a field emission electron probe micro-analyzer (FE-EPMA: JEOL JXA-8500F)
133 equipped with five wavelength-dispersive spectrometers. Methods of the EMP analysis were
134 previously described (Zhang et al. 2012). In addition, we studied > 400 thin sections of the
135 ophiolite complex recovered from a pilot-hole at Luobusa. In order to search for diamond, in

cases where it was not present on the surface by binocular and petrographic microscopes, the mounts were polished and re-polished repeated several times for each sample employing a Buehler Phoenix Beta Twin plate/Polisher (Yang et al. 2015). Where *in situ* diamond seemed to be present, microprobe, SEM and Laser Raman spectroscope studies were carried out to confirm its presence. Yang's CAGS group checked ~40 disc samples. In all, the group found four in *situ* diamond inclusions in chromite from the Luobusa chromitite. During this procedure, the mounts did not come in contact with a diamond saw or any other diamond-bearing materials, thus, excluding the possibility of contamination**.**

LUOBUSA OPHIOLITE AND CHROMITITE

Luobusa ophiolite

The lithological profile of the pilot-hole (LSD-1, 1478.8 m) indicates that the Luobusa ophiolite consists of three overturned units: mantle tectonite, mantle-crust transition zone, and crustal cumulate (authors' unpublished research). The tectonite unit (0-1207 m) is chiefly harzburgite with numerous layers and lenses 2-20 m thick of lherzolite and dunite. The transition zone (1207-1412 m) between tectonite and cumulate consists of fresh dunite 194 m thick with or without minor clinopyroxenite and diabase. The cumulate (1412-1478.8 m) unit consists exclusively of gabbro; comagmatic pillow lava and a capping layer of chert crop out on the surface.

Harzburgitic and lherzolitic tectonites consist of variable amounts of coarse-grained olivine (Fo_{89-90}), enstatite (En_{90}), Cr-bearing diopside (Cr_2O_3: 0.61-0.92 wt%) and spinel ± rare pentlandite and FeNi alloys; these phase assemblages exhibit granular or porphyroclastic textures. All coarse-grained enstatite crystals in the peridotites contain abundant clinoenstatite

159 and diopside lamellae. With a few exceptions, spinel grains in lherzolite and harzburgite have
160 variable Mg# (Mg/Mg+Fe) of 0.57-0.78, Cr# (Cr/Cr+Al) of 0.17-0.39, and very low TiO_2 (<
161 0.2 wt%). Dunite of the tectonite unit consists of olivine (> 90 vol%, Fo_{91-92}) and chromite (< 5
162 vol%) ± enstatite, and shows granular to porphyroclastic textures. Olivine is coarse-grained,
163 from 2 mm to > 5 cm and displays kink bands. Chromite grains have lower Mg-# (0.39-0.63)
164 and higher Cr-# (0.65-0.89) than chromite in the mantle peridotites.
165
166 **Podiform chromitites**
167 Podiform chromitites occur as lenses 20-250 m long and 0.5-5 m thick, as massive layers
168 0.5-3 m thick, irregular masses up to 20 m thick, and as veins within harzburgites. The ore
169 district is 6.5 km long and 2.3 km wide. Most podiform chromitites display a dunite envelope
170 several centimeters to several meters thick surrounded by harzburgite. Podiform chromitites
171 are mainly magnesiochromite (Mg-Chr), associated with forsterite ± diopside, and exhibit
172 massive (Fig. 2a), nodular (Fig. 2b), disseminated (Fig. 2c), and brecciated textures. These
173 textures lack sharp boundaries (Fig. 2d). Olivine, near-end-member forsterite (Fo_{96-98}), contains
174 elevated NiO (0.42-1.31 wt.%) and variable Cr_2O_3 (up to 1.07 wt.%). Most Mg-Chr grains are
175 chemically homogenous and have high Cr/(Cr+Al) and Mg/(Fe+Mg) ratios of 0.77-0.84 and
176 0.70-0.76, respectively. Average $Fe^{3+}/\sum Fe$ ratios of the chromite range from 0.22 to 0.32,
177 based on charge balance, for 9 EPMA samples. Some grains exhibit a thin chromite rim with
178 extremely high Cr# 0.90-0.97 and low Mg# 0.60-0.69 that formed at shallow depths. In
179 addition to diamond (Fig. 2e), the chromite contains inclusions of olivine, diopside, metal
180 alloys, native elements, brucite and FeNi sulfides. Some possible non-UHP phases, such as Cr-
181 Na-bearing pargasite, an unidentified Al-rich mineral, and hydrous phases with variable Si-Cr-

Fe-Mg compositions are also present as inclusions in chromite. Most olivine inclusions in chromite are partially replaced by lizardite/antigorite, Cr-bearing chlorite and tiny blebs of secondary FeNi alloys. Based on the contrasting inclusion assemblages, associated UHP polymorphs, and chromite textures, the chromites may have formed at different mantle depths. Olivine contains inclusions of moissanite, chromite, wüstite, native Fe and FeNi alloys (see following section).

IN SITU MATERIAL IDENTIFICATION

We now describe newly recognized *in situ* SuR UHP phases, native elements, and metal alloys in disseminated chromitites (Fig. 2c).

Moissanite (i.e., natural SiC)

Moissanite crystals differ from silicon carbide in the polishing papers in both color and size, which rules out contamination due to sample preparation. Many moissanite crystals in chromitite sample YK15A are blue, granular or prismatic grains tens to ~200 μm in diameter (Fig. 3a). They occur as inclusions in olivine or as an interstitial phase in olivine domains (Fig. 3b). The distinct Raman bands at 788 and 969cm^{-1} are consistent with those of the moissanite standard (Fig. 3c).

Native (i.e., metallic) Si and Fe, and wüstite

Native Si and Fe occur together in a composite inclusion pocket in chromite from a disseminated chromitite (YX18B); native Fe is present in olivine from sample 13YK15A. Native Si is also reported as inclusions in moissanite recovered from chromitites (Robinson et

al. 2004). Native Si on the surface is rounded or leaf-like with variable dimensions (2-8μm) (Fig. 4a), and shows a strong Si peak in the energy dispersive X-ray (EDX) spectrum (Fig. 4b). Native Fe is rounded or flake-like, 2-3 μm in diameter (Fig 4a). It has a strong Feα peak in its EDX spectrum (Fig. 4c). The native Fe is nearly pure iron, but contains minor Si at its margin (see Fig. Al element maps); it appears that a Fe-Si phase locally replaced the native Fe along its margin.

We recognized wüstite by EDX spectra and X-ray element mapping (Fig. 5). It is euhedral, ~ 2 μm across, and is associated with an unknown W-Ca-Si-O phase, native Fe, moissanite and an FeNi alloy in a 40 x 60 micrometer domain within olivine in sample YK15A (Fig. 3b).

FeNi alloys

Primary FeNi alloys occur in the Luobusa chromitites as interstitial crystals between chromite grains, and as inclusions in chromite and olivine (Figs. 6a, b, c). The FeNi alloys exhibit plate-like or rounded shapes, and range in size from several to > 100 μm. Their main component is Ni (Cr_{0-2}-$Fe_{7-20}Ni_{78-93}$, Table 1). In addition, secondary FeNi alloys together with hydrous phases are common as tiny grains in serpentine after olivine, or as relatively coarser fracture fillings. Rare FeCr alloy inclusions in chromite (Figs. 6d, e) and olivine contain very minor Mn; a TiC alloy is rarely present at the olivine margins (see Fig. 3d).

Minerals of crustal origin

Asphaltum and hexagonal boron nitride (h-BN) occur as minute inclusions in a chromite crystal from sample YK15B. Their Raman spectra are compatible with standards: asphaltum

227 shows two broad peaks at 1350 and 1590 cm^{-1} (Fig. 7a); h-BN has a strong peak at 1364 cm^{-1}
228 (Fig. 7b).

229

230 ## DISCUSSION

231

232 ### Moissanite formation

233 Moissanite (SiC) is a rare super-reducing mineral that has been reported in meteorites, in
234 close spatial association with diamond in kimberlites and eclogites, in ophiolitic podiform
235 chromitites and in peridotites (for review, see Hazen et al. 2013). In our study, moissanite in
236 the diamond-bearing Luobusa chromitite is associated with or occurs as inclusions in olivine;
237 the olivine also contains inclusions of wüstite + native Fe (Fig. 3b). Reactions producing
238 moissanite may be expressed by the following:

239 $$SiC + O_2 = C + SiO_2 \quad (1)$$

240 $$SiC + Mg_2SiO_4 + O_2 = C + 2MgSiO_3 \quad (2)$$

241 Woermann and Rosenhauer (1985) calculated the log fO_2–T redox stability of SiC for reaction
242 (2) with $\log fO_2 = 8.307 - 44635/T + 0.2841 \log T + 0062P/T$ (P in bars, T in K, and assuming
243 constant ΔV(solid). Reaction (2) is compatible with a moissanite-bearing assemblage for the
244 Luobusa chromitite. Experiments at 1.5 and 9.0 GPa and 1300-1500 ^oC by Ulmer et al. (1998)
245 indicated that the formation of moissanite - olivine was only observed in run U1062 at 9.0 GPa
246 and 1300 ^oC using a starting assemblage of VO/ZrO_2/(Opx + C) with very low oxygen fugacity
247 (Log fO_2 = -15.9 bar). Similarly, Dobrzhinetskaya and Green (2007) produced moissanite in
248 their diamond synthesis experiments at 1450-1500 ^oC, 8.5 GPa. These experiments suggested

249 that formation of moissanite requires a pressure of at least 8.5 - 9 GPa in diamond-bearing
250 rocks.

251 The occurrence of moissanite and associated SuR assemblages suggests that crystallization
252 occurs under extremely reducing conditions. Moissanite stability requires oxygen fugacities
253 several orders of magnitude lower than that of the IW buffer (Essene and Fisher 1986; Frost
254 and McCammon 2008; Mathez et al. 1995; Schmidt et al. 2014; Ulmer et al. 1998; Woodland
255 and Koch 2003). Accordingly, deep-origin hypotheses have been proposed, such as moissanite
256 being a remnant from a primordial ultra-reduced mantle or from the core-mantle boundary
257 (Mathez et al. 1995), having a possible lower mantle origin for those from Luobusa ophiolitic
258 chromitite (Trumbull et al. 2009), being stable in the *P*-*T* fields of diamond and molten Si from
259 kimberlite (Shiryaev et al. 2011), and representing one of the deepest mantle minerals known
260 to have reached the surface (Hazen et al. 2013). In contrast, Schmidt et al. (2014) considered
261 that formation near the core-mantle boundary or the lower mantle should be ruled out on the
262 basis of temperature, because moissanite cannot survive at very high temperature.

263 Redox conditions in the mantle may not be homogeneous (Ulmer et al. 1998; McCammon
264 2005). Rocks in the deep upper mantle are likely to be reduced relative to the fayalite-
265 magnetite-quartz (FMQ) buffer (e.g., Ballhaus 1995; Woodland and Koch 2003). Ulmer et al.
266 (1998) also hypothesized that low fO_2 conditions must exist somewhere in the upper mantle,
267 which would permit moissanite to crystallize and survive. Moreover, oxygen fugacities more
268 reducing than IW in the deep upper mantle have been suggested to account for platinum-group
269 element fractionation between a partial melt and its mantle residue (Ballhaus 1995). In
270 summary, the ultimate source of moissanite in ophiolitic chromitites is not definitely known,
271 but the mantle transition zone, and/or possible deep upper mantle origin is a distinct possibility.

272

273 **Native Fe formation and redox conditions of SuR assemblages**

274 As described above, *in situ* super-reducing phases in the Luobusa chromitites include
275 diamond, moissanite, wüstite, native Fe and Si, as well as FeNi alloys. Except for diamond,
276 these phases chiefly occur in meteorites, but are rare in terrestrial rocks. Previous studies
277 indicated that oxygen fugacity is relatively high (near the fayalite-magnetite-quartz buffer) at
278 the top of the upper mantle due to the concentration of Fe^{3+} in modally minor phases; however
279 fO_2 decreases significantly with depth. At the 410 km discontinuity, redox conditions lie below
280 the iron-wüstite buffer (Woodland and Koch 2003). Thus, fO_2 is near iron metal equilibrium in
281 the MTZ and in the lower mantle (McCammon 2005). The relatively high oxygen fugacities of
282 the upper mantle would destabilize the SuR phases (Hirsch 1991; Mathez et al. 1995). The
283 formation of native Fe in the Luobusa chromitites may be related to the existence of high Fe^{3+}
284 content in chromite and equlibium of moissanite and olivine. Average $Fe^{3+}/\sum Fe$ ratios of
285 chromites are 0.22-0.32 for Luobusa chromitite samples, and the Fe^{3+} contents are generally
286 though to be underestimated in comparision with those measured directly by Mössbauer
287 spectroscopy (Quintiliani et al. 2006; Ruskov et al. 2010). High concentration of Fe^{3+} occurs
288 even under highly reducing conditions, and charge balance at low fO_2 occurs through
289 disproportionation ($3Fe^{2+} = Fe^0 + 2Fe^{3+}$), where iron metal is formed in discrete blebs (Frost et
290 al. 2004; Lauterbach et al. 2000). Moissanite is a SuR phase formed under oxygen fugacities
291 significantly below fO_2 values defined by the IW buffer (Frost and McCammon 2008, Ulmer et
292 al. 1998). At such low oxygen fugacities, most Fe^{2+} should be reduced to metal. Ni-rich FeNi
293 alloys probably are also formed in such reducing conditions. Thus coexisting mantle phases
294 such as olivine and orthopyroxene should have unusually high X_{Mg} values (Schmidt et al.

295 2014). This is consistent with observations in the Luobusa chromitite where moissanite and
296 native Fe are present as inclusions in high X_{Mg} olivine (Fo_{96-98}), or are intimately associated
297 with the olivine.
298
299 **SuR UHP assemblages from the Luobusa chromitites: A window on the deep upper**
300 **mantle and MTZ**
301
302 Diamond is well known in kimberlites/lamproites, peridotites, mantle eclogites, and UHP
303 metamorphic rocks. Most diamond crystals formed at high *T* and *P* at minimum depths of 130-
304 250 km (Cartigny 2005; Sobolev and Shatsky 1990; Zhang et al. 1997). Exceptional cases
305 evoke the possibility of crystallization in the MTZ or lower mantle based on studies of mineral
306 inclusions in kimberlitic diamonds (Cartigny 2005; Stachel et al. 2005). Occurrences include
307 documented or inferred inclusions of majorite, ferropericlase, stishovite, TAPP (a tetragonal
308 almandine-pyrope phase), MgSi- and CaSi-perovskite (Stachel et al. 2000, 2005), wüstite,
309 native Fe (Wirth et al. 2009) in diamond, and in ultradeep xenoliths (Haggerty and Sautter
310 1990). Except for a few reports, UHP minerals from the deepest upper mantle, MTZ and the
311 lower mantle are extremely rare, presumably because of widespread back reaction on
312 decompression.
313 In addition to diamond (~200 μm in Fig. 2e, as well as separated grains 200-500 μm in size
314 described by Yang et al. 2014) and moissanite in the Luobusa chromitites, wüstite and FeNi
315 alloys also occur in the Luobusa chromitites. An iron-rich FeNi alloy is the main component in
316 the Earth's core (Birch 1952; McDonough and Sun 1995), and also occurs as inclusions in
317 kimberlitic diamond. Wüstite and primary FeNi alloys are thought to be stable in the lower

mantle (Birch 1952; McCammon 2005). Similarly, diamond associated with inferred stishovite probably also was derived from the MTZ. Mineralogical/chemical characteristics of the chromitite suggest that diamond, moissanite and associated highly reduced assemblages formed under the low fO_2 environment of the MTZ and possible in the adjacent upper mantle; this conclusion is supported by the co-existence of associated wüstite and inferred ringwoodite. *In situ* identification of SuR UHP assemblages in the Luobusa chromitites demonstrates that these phase associations do not reflect contamination. Thus, diamond-bearing chromitites in ophiolitic suture zones provide new constraints on the multistage formation of ophiolitic podiform chromitites, and on the *P-T* compositional evolution and redox environment of the deep upper mantle and MTZ.

Recycling of crustal materials

Asphaltum is of clear crustal origin, and occurs in porous sediments or as inclusions in minerals of the sedimentary strata. Natural cubic boron nitride (c-BN) was first found in a ball-like aggregate recovered from a Luobusa chromitite, and occurs as inclusions in TiN, and in coesite (Dobrzhinetskaya et al. 2009) that was inferred to have replaced stishovite (Yang et al. 2007). Qinsongite (i.e., c-BN) apparently formed through reaction of crustal boron, originally stored in mica or clay in a deeply subducted pelitic rock, with mantle nitrogen, then was exhumed by entrainment in chromitite (Dobrzhinetskaya et al. 2014). The natural hexagonal form of boron nitride (h-BN) has the same chemical origin as c-BN, but crystallized under lower *P-T* conditions. The presence of asphaltum and h-BN along with previous reported crustal minerals, especially ancient zircon grains of continental origin, suggests derivation from

crustal materials including metasedimentary rocks that were recycled into the mantle through subduction. Some grains may have been included in the chromite by precipitation from rising asthenospheric and suprasubduction-zone magmas (Robinson et al. 2015), and are metastably preserved.

Both diamond and moissanite separates from the Luobusa chromitites have distinct ^{13}C-depleted isotopic compositions (δ^{13}C from -18 to -35 ‰ for diamond, -22 to -32‰ for moissanite), which is much lighter than the dominant mantle carbon reservoir (δ^{13}C = -5‰; Trumbull et al. 2009). The distinctive low δ^{13}C values of associated diamond + moissanite likely reflect a metasedimentary carbon source derived from mixtures of organic matter and carbonate. This metasedimentary carbon undoubtedly returned to the mantle via subduction (Cartigny 2009). Trumbull et al. (2009) proposed a similar origin. There authors indicated that isotopic fractionation from the mantle carbon reservoir with a δ^{13}C value of -5‰, with or without Rayleigh distillation cannot explain the ^{13}C-depleted range of moissanite. Subduction of biogenic carbonaceous material, however, does satisfy both the unusual isotopic and redox constraints on moissanite formation. The initial carbon source of the low δ^{13}C values of diamond (including kimberlitic diamond) and moissanite remains under debate, but many studies support the hypothesis that extremely light carbon isotopic compositions of these phases reflect deep mantle recycling of crust materials (e.g., Cartigny, 2009; Trumbull et al. 2009; Walter et al. 2011; Wirth et al. 2009). Another possibility is that the low δ^{13}C values of diamond and moissanite reflect derivation from reduced fluids originating from metamorphosed organic carbon (Schmidt et al. 2014). Low δ^{13}C values of diamond and moissanite combined with the existence of c-BN in an inferred stishovite suggest the insertion of crustal materials into the deep Earth, including the MTZ. The suboceanic mantle thus may

364 be more heterogeneous than previously thought. This is consistent with seismic tomographic
365 studies demonstrating that lithospheric slabs can be subducted to the MTZ or deeper, and
366 possibly accumulate at the mantle-core boundary (Fukao 2001).
367
368 **IMPLICATIONS**
369 Early identification of SuR UHP minerals was obtained on grains separated from very large
370 samples of chromitite. The true nature of the separated minerals in chromitite is problematic
371 due to possible contamination during sample preparation. Newly identified *in situ* SuR UHP
372 and associated SuR phases occur as inclusions in chromite and olivine in Luobusa ophiolitic
373 podiform chromitites, proving that these SuR phases are not exotic contaminants. These
374 findings require that the SuR UHP assemblage of diamond, moissanite, wüstite, primary FeNi
375 alloys, and associated native Fe and Si initially formed under a highly reducing environment
376 likely in the mantle transition zone. Diamond and moissanite with distinct, low ^{13}C-depleted
377 isotopic compositions probably reflect a metasedimentary carbon source; low-*P* crustal
378 minerals as xenocrysts metastably persist in the chromitites, demonstrating that these materials
379 including carbon-bearing metasedimentary rocks were recycled into the mantle.
380 Four models have recently been proposed to explain the origin of diamond-bearing
381 chromitites: (1) deep recycling (Arai 2013); (2) deep subduction (MaGowan et al. 2015); (3)
382 deep-seated mantle plumes (Yang et al. 2015); and (4) shallow origin-hydrous mafic magma
383 models (Zhou et al. 2014). Based on petrological and mineralogical characterizations and
384 available geochronological data of chromitites and host mantle harzburgites, we propose an
385 alternative 3-stage model.

386 (1) Stage I: Shallow-crustal formation of the Luobusa ophiolite occurred. Mineralogical
387 and chemical characteristics of the harzburgite indicate that it is a remnant of oceanic
388 lithosphere subjected to a moderate degree of partial melting and melt expulsion. The
389 ophiolite evidently formed at a mid-ocean ridge at 162.9±2.8 Ma, as indicated by U-Pb
390 SHRIMP dating of zircon from comagmatic diabase dikes (Zhong et al. 2006).

391 (2) Stage II: Chromitite formation attended intra-oceanic lithospheric slab subduction to
392 profound mantle depths. The production of a slab window at ca. 120-160 km occurred due to
393 breakoff of the downgoing oceanic lithosphere, allowing upwelling and decompression
394 melting of the underlying asthenosphere. The resultant magmas formed in the MTZ (and deep
395 upper mantle) under a highly reducing environment, and contained ringwoodite, SuR UHP
396 minerals such as diamond, moissanite, wüstite, various metal alloys, and UHP chromite with
397 inferred CF structure. During crystallization of the Cr-rich magma, chromite formed and
398 encapsulated these SuR UHP materials.

399 (3) Stage III: UHP chromite-bearing melt then rose though the mantle wedge and
400 reacted with uppermost mantle peridotites, subsequently precipitating additional chromitite at
401 about 120 ± 10 Ma (Yamamoto et al., 2013) in a suprasubduction zone environment.

402 In summary, discoveries of diamond and other SuR UHP phases in ophiolitic podiform
403 chromitites in the Yarlung Zangbo suture zone, Tibet, as well as in the Polar Urals, and in
404 Myanmar imply the existence of a new type of chromitite. Such mineral assemblages provide
405 an additional way to explore the physical-chemical conditions of the deep upper mantle and
406 MTZ, mantle dynamics, as well as the profound recycling of crustal materials.

407

408 **ACKNOWLEDGMENTS**

This research was supported by the State Key Laboratory of Continental Tectonics and Dynamics, Institute of Geology, Chinese Academy of Geological Sciences, Beijing, and the Ministry of Science and Technology (formerly, National Science Council) of Taiwan. We appreciate the help of Yu-shiang Wang, concerning Hui-ho Shieh and Ling Yan for SEM, electron microprobe and Raman spectra analyses, respectively. We thank J. G. Liou for a helpful review on an early version of this manuscript. Finally we appreciate Thomas Stachel and Yoshihide Ogasawara for their critical review, and thank Jane A. Gilotti for her editorial correction for revision.

REFERENCES CITED

Arai, S. (2013) Conversion of low-pressure chromitites to ultrahigh-pressure chromitites by deep recycling: A good inference. Earth and Planetary Science Letters, 379, 81-87.

Bai, W.J., Zhou, M.F., and Robinson, P.T. (1993) Possible diamond-bearing mantle peridotites and chromitites in the Luobusa and Dongiao ophiolites, Tibet. Canadian Journal of Earth Sciences, 30, 1650-1659.

Bai, W.J., Robinson, P.T., Fang, Q.S., Yang, J.S., Yan, B., Zhang, Z., Hu, X.-F. Zhou, M.-F., and Malpas, J. (2000) The PGE and base-metal alloys in the podiform chromitites of the Luobusha ophiolite, southern Tibet. The Canadian Mineralogist, 38, 585-598.

Bai, W.J., Yang, J.S., Fang, Q.S., Yan, B.G., and Shi, R.D. (2003) An unusual mantle mineral group in ophiolites of Tibet. Chinese Geology, 30, 144-15 (in Chinese with English abstract).

Birch, F. (1952) Elastical and constitution of the Earth's interior. Journal of Geophysics Research, 57, 227-286.

Ballhaus C. (1995) Is the upper mantle metal-saturated? Earth and Planetary Science Letters, 132, 75-86.

Cartigny, P. (2005) Stable isotopes and the origin of diamond. Elements, 1, 79-84.

_____ (2009) Volatile composition of microinclusions in diamonds from the Panda kimberlite, Canada: Implications for chemical and isotopic heterogeneity in the mantle. Geochimica et Cosmochimca Acta, 73, 1779-1794.

Coleman, R.G. (1977) Ophiolites-Ancient Oceanic Lithosphere? Springer-Verlag Berlin, Heidelberg, New York.

Dilek, Y., and Furnes, H. (2014) Ophiolites and their origins. Elements, 10, 2-9.

Dobrzhinetskaya, L.F., and Green, H.W. (2007) Diamond synthesis from graphite in the presence of water and SiO_2: implications fro diamond formation in quartzites from Kazakhstan. International Geology Review, 49, 389-400.

Dobrzhinetskaya, L.F., Wirth, R., Yang, Y.J., I. D. Hutcheon, I.D., Weber, P.K., and Green, H.W. (2009) High-pressure highly reduced nitrides and oxides from chromitite of a Tibetan ophiolite. Proceedings of the National Academy of Sciences, 106, 19233–19238.

Dobrzhinetskaya, L.F., Wirth, R., Yang, Y.J., Green, H.W., Hutcheon, I.D., Weber, P.K., and Grew, E.S. (2014) Qingsongite, natural cubic boron nitride: the first boron mineral from the Earth's mantle. American Mineralogist, 99, 764-772.

Essene, E.J., and Fisher, D.C. (1986) Lightning strike fusion: extreme reduction and metalsilicate liquid immiscibility. Science 234, 189–193.

Frost, D.J., Liebske, C., Langenhorst, F., McCammon, C.A., Trønnes, R., and Rubie, D.C. (2004) Experimental evidence for the existence of iron-rich metal in the Earth's lower mantle. Nature, 428, 409-411.

455 Frost, D.J., and McCammon, C.A. (2008) The Redoc state of Earth's mantle. Annual Review of
456 Earth Planet Sciences, 36, 389-420.
457 Fukao, Y., Widiyantoro, S., and Obayashi, M. (2001) Stagnant slabs in the upper and lower
458 mantle transition region. Reviews of Geophysics, 39, 291-323.
459 Haggerty, S.E., and Sautter, V. (1990) Ultradeep (greater than 300 kilometers), ultramafic upper
460 mantle xenoliths. Science, 248, 993-996.
461 Hazen, R.M., Downs, R.T., Jones, A.P., and Kah, L. (2013) Carbon mineralogy and crystal
462 chemistry. Reviews of Mineralogy and Geochemistry, 75, 7-46.
463 Hirsch, L.M. (1991) The Fe-FeO buffer at low mantle pressures and temperatures. Geophysical
464 Research letters, 18, 1309-1312.
465 Ishii, T., Kojitani, H., Fujino, K., Yusa, H., Mori, D., Inaguma, Y., Matsushita, Y., Yamaura,
466 K., and Akaogi, M. (2015) High-pressure high-temperature transitions in $MgCr_2O_4$ and
467 crystal structures of new $MgCr_2O_5$ and post-spinel $MgCr_2O_4$ phases with implications for
468 ultrahigh-pressure chromitites in ophiolites. American Mineralogist, 100, 59-65.
469 Lauterbach, S., McCammon, C.A., Aken, P. van., Langenhorst, F., and Seifert, F. (2000)
470 Mössbauer and ELNES spectroscopy of $(Mg,Fe)(Si,Al)O_3$ prerovskite: A highly oxidized
471 component of the lower mantle. Contributions to Mineralogy and Petrology, 138, 17-26.
472 Liou, J.G., Tsujimori, T., Yang, J.S., Zhang, R.Y., and Ernst, W.G. (2014) Recycling of crustal
473 material through study of ultrahigh-pressure minerals in collisional orogens, ophiolites, and
474 mantle xenoliths: A review. Journal of Asian Earth Sciences, 96, 386-420.
475 Malpas, J., Zhou, M.F., Robinson, P.T., and Reynolds, P.H. (2003) Geochemical and
476 geochronological constraints on the origin and emplacement of the Yarlung-Zangbo

ophiolites, southern Tibet. Special Publications (Geological Society, London), 218, 191-206.

McGowan, N.M., Griffin, W.L., González-Jiménez, J.M., Belousova, E., Afonso, J. C., Shi, R., McCammon, C.A., Pearson, N.J., and O'Reilly, S.Y. (2015) Tibetan chromitites: Excavating the slab graveyard. Geology, 43, 179-182.

Mathez, R.A., Fogel, E.A., Hutcheon, I.D., and Marshintsev, V.K. (1995) Carbon isotope composition and origin of SiC from kimberlites of Yakutia, Russia. Geochimica et Cosmochimica Acta, 59, 781–791.

McCammon, C.A. (2005) Mantle Oxidation State and Oxygen Fugacity: Constraints on mantle chemistry, structure, and Dynamics. Earth's deep mantle: structure, composition, and Evolution. Geophysical Monograph Series, 160, 219-240.

McDonough, W.F., and Sun S.S. (1995) The composition of the Earth. Chemical Geology, 120, 223-253.

Quintiliani, M., Andreozzi, G.B, and Graziani, G. (2006) Fe2+ and Fe3+ quantification by different approaches and fO2 estimation for Albanian Cr-spinel. American Mineralogist, 91, 907-916.

Robinson, P.T., Bai, W.J., Malpas, J., Yang, J.S., Zhou, M.F., Fang, Q.S., Hu, X.F., Cameron, S., and Staudigel, H. (2004) Ultra-high pressure minerals in the Luobusa ophiolite, Tibet, and their tectonic implications. Special Publications (Geological Society, London), 226, 247-271.

Robinson, P.T., Trumbull, R.B., Schmitt, A., Yang, J.S., Li, J.W., Zhou, M-F., Erzinger, J., Dare, S., and Xiong, F-H. (2015) The origin and significance of crustal minerals in ophiolitic chromitites and peridotites. Gondwana Research, 27, 487-506.

Ruskov, T., Spirov, I., Georgieva, M., Yamamoto, S., Green, H.W., McCammon, C. A., and Dobrzhinetskaya, L.F. (2010) Mossbauer spectroscopy studies of the valence state of iron in chromite from the Luobusa massif of Tibet: implications for a highly reduced deep mantle. Journal of Metamorphic Geology, 28, 551-560.

Schmidt, M.W., Gao, C., Golubkova, A., Rohrbach, A., and Connolly, J.A.D. (2014) Natural moissanite (SiC) – a low temperature mineral formed from highly fractionated ultra-reducing COH-fluids. Progress in Earth and Planetary Science, 127, 279-307.

Shiryaev, A.A., Griffin, W.L., and Stoyanov, E. (2011) Moissanite (SiC) from kimberlites: polytypes, trace elements, inclusions and speculation on origin. Lithos, 122, 152-164.

Sobolev, N.V., and Shatsky, V.S. (1990) Diamond inclusions in garnets from metamorphic rocks: a new environment for diamond formation. Nature, 343, 742-746.

Stachel, T., Brey, G.P., Harris, J.W., 2000. Kankan diamonds (Guinea) I: from the lithosphere down to the transition zone. Contributions to Petrology and Mineralogy, 140, 1-15.

Stachel, T., Brey, G.P., and Harris, J.W. (2005) Inclusions in sublithospheric diamonds: Glimpses of deep earth. Elements 1, 73-78.

Trumbull, R.B. Yang, J.S., Robinson, P.T., Pierro, S. Di., Vennemann, T., and Wiedenbeck, M. (2009) The carbon isotope composition of natural SiC (moissanite) from the Earth's mantle: New discoveries from ophiolites. Lithos, 113, 612-620.

Ulmer, G., Grandstaff, D.E., Woermann, E, Göbbels, M., Schönitz, M., and Woodland, A.B. (1998) The redox stability of moissanite (SiC) compared with metal-metal oxide buffers at 1773 K and at pressures up to 90 kbar. Neues Jahrbuch für Mineralogie-Abhandlungen, 172, 279-307.

Walter, M.J., Kohn, S.C., Araujo, D., Bulanova, G.P., Smith, C.B., Gillou, E., Wang, J., Steele, A., and Shirey, S.B. (2011). Deep mantle cycling of oceanic crust: evidence from diamonds and their mineral inclusions. Science, 334, 54-57.

Whitney, D.L., and Evans, B. (2010) Abbreviations for names of rock-forming minerals. American Mineralogist, 95, 185-187.

Wirth, R., Kamincky, F., Matsuk, S., and Schreiber, A. (2009) Unusual micro- and nano-inclusions in diamond from the Juina area, Brazil. Earth and Planetary Science Letters, 286, 292-303.

Woermann, E. and Rosenhauer, M. (1985) Fluid phases and the Redox State of the Earth's Mantle: Extrapolation based on experimental, phase-theoretical and petrological data. Fortschritte der Mineralogie, 63, 263-349.

Woodland, A.B. and Koch, M. (2003) Variation in oxygen fugacity with depth in the upper mantle beneath the Kaapvaal craton, Southern Africa. Earth and Planetary Science Letters, 214, 295-310.

Xiong, F.H., Yang, J.S., Robinson, P.T., Xu, X.Z., Liu, Z., Li, Y., Li, J.Y., and Chen, S.Y. (2015) Origin of podiform chromitite, a new model based on the Luobusa ophiolite, Tibet. Gondwana Research, 27, 525-542.

Xu, X.Z., Yang, J.S., Chen, S.Y., Fang, Q.S., Bai, W.J., and Ba, D.Z. (2009) Unusual mantle mineral group from chromitite ore body Cr-11 in Luobusa ophiolite of the Yarlung-Zangbo suture zone, Tibet. Journal of Earth Sciences, 20, 284-302.

Xu, X.Z., Yang, J.S., Robinson, P.T., Xiong, F.H., Ba, D.Z., and Guo, G.L. (2015) Origin of ultrahigh pressure and highly reduced minerals in podiform chromitites and associated mantle peridotites of the Luobusa ophiolite, Tibet. Gondwana Research, 27, 507-524.

Yamamoto, S., Komiya, T., Hirose, H., and Maruyama, S. (2009) Coesite and clinopyroxene exsolution lamellae in chromites: In-situ ultrahigh-pressure evidence from podiform chromitites in the Luobusa ophiolite, southern Tibet. Lithos, 109, 314-322.

Yamamoto, S., Komiya, T., Yamamoto, H., Kaneko, Y., Terabayashi, M., Katayama, I., Iizuka, T., Maruyama, S., Yang, J.S., Kon, Y., and Hirata, T. (2013) Recycled crustal zircons from podiform chromitites in the Luobusa ophiolite, southern Tibet. The Island Arc, 22, 89-103.

Yang, J.S., Dobrzhinetskaya, L., Bai, W.J., Fang, Q.S., Robinson, P.T., Zhang, J.F., and Green, II, H.W. (2007) Diamond- and coesite-bearing chromitites from the Luobusa ophiolite, Tibet. Geology, 35, 875-878.

Yang, J.S., Robinson, P.T., and Dilek, I. (2014) Diamonds in ophiolite. Element, 10, 127-130.

Yang, J.S., Meng, F.C., Xu, X.Z., Robinson, P.T., Dilek, Y., Makeyev, A.B., Wirth, R., Wiedenbeck, M., Griffin, W.L., and Cliff, J. (2015) Diamonds, native elements and metal alloys from chromitites of the Ray-Iz ophiolite of the Polar Urals. Gondwana Research, 27, 459-485.

Zhang, R.Y., Liou, J.G., Ernst, W.G., Coleman, R.G., Sobolev, N.V. and Shatsky, V.S. (1997) Metamorphic evolution of diamond-bearing and associated rocks from the Kokchetav Massif, northern Kazakhstan. Journal of Metamorphic Geology, 15, 479-496.

Zhang, R.Y., Liou, J.G., Omori, S., Sobolev, N.V., Shatsky, V.S., Iizuka, Y., Lo, C-H., and Ogasawara, Y. (2012) Tale of the Kulet eclogite from the Kokchetav Massive, Kazakhstan: Initial tectonic setting and transition from amphibolite to eclogite. Journal of Metamorphic Geology, 30, 537-559.

Zhong, L.F., Xia, B., Zhang, Y.Q., Wang, R., Wei, D.L., and Yang, Z.Q. (2006) SHRIMP age determination of the diabase in Luobusha ophiolite, southern Xizang (Tibet). Geological Review, 52, 224-229 (in Chinese with English abstract).

Zhou, M.F., Robinson, P.T., Malpas, J., and Li, Z. (1996) Podiform chromitites in the Luobusa ophiolite (southern Tibet): Implications for melt-rock interaction and chromite segregation in the upper mantle. Journal of Petrology, 37, 3-21.

Zhou, M.F., Robinson, P.T., Malpas, J., Edwards, S.J., and Qi, L. (2005) REE and PGE geochemical constraints on the formation of dunites in the Luobusa ophiolite, southern Tibet. Journal of Petrology, 46, 615-639.

Zhou, M.F., Robinson, P.T., Su, B-X., Gao, J., Li, W., Yang, J-S., and Malpas, J. (2014) Compositions of chromite, associated minerals, and parental magmas of podiform chromite deposits: The role of slab contamination of asthenospheric melts in suprasubduction zone environments. Gondwana Research, 26, 262-283.

Figure captions

FIGURE 1. Distribution of ophiolites along the Yarlung-Zangbo suture zone, and Luobusa podiform chromitites, Tibet. a) Regional location of the Luobusa ophiolite. b) Simplified geological map of the Luobusa area showing three chromitite deposits (Kanjinla, Xiangkashan, and Luobusa).

FIGURE 2. Photographs and characteristic X-ray images showing occurrences and textures of chromitite, as well as a diamond inclusion in chromite. a) Banded, massive chromitite in harzburgite from Xiong et al. (2015). b) Nodular chromitite: dark chromite

590 nodules in olivine matrix. c) Scan of a polished thin section of chromitite (YK15) showing
591 intensely disseminated texture. d) Massive and disseminated textures are gradational. e) Cr
592 and C mapping of a diamond inclusion in chromite from a Luobusa chromitite (Yang et al.
593 2014 reported, but did not illustrate this occurrence). Amor C, amorphous carbon. Mineral
594 abbreviation after Whitney and Evans (2010). Chr, chromite; Dia, diamond; Ol, olivine.

595 **FIGURE 3.** Occurrences and Raman spectrum of moissanite. a) Photograph of part of
596 polished rock chip, taken under binocular microscope. Blue moissanite grains occur as
597 inclusions in olivine, and as an interstitial phase between olivine grains. In the image, most
598 moissanite grains are under the surface, but the margins of a few grains are exposed. Reflected
599 light (YK15A, discs of a polished rock chip from sample YK15). b) Backscattered electron
600 image shows a multiple inclusion domain in olivine, and a large moissanite crystal; most parts
601 of which lie beneath the surface, with only its margins exposed. c) Raman spectrum of
602 moissanite (Moi) shown in (b). (d) Enlarged view of the multiple inclusions in olivine,
603 containing inclusions of wüstite, native Fe, FeNi alloys, and an unknown phase (for details,
604 see figure. 5).

605 **FIGURE 4.** Backscattered electron (BSE) image of inclusions in chromite. a) Mulitple
606 inclusions of native Si, Fe and olivine in chromite. b, c) Energy dispersive X-ray (EDX)
607 spectra of native Si and Fe; weak peaks of Mg, Si and Cr are from nearby chromite and
608 olivine.

609 **FIGURE 5.** SEM-BSE image and X-ray maps of Fe, O, Si, Ca and W of wüstite
610 (Wus) and an associated unknown phase (outlined in red), consisting chiefly of W, Ca, Si
611 and minor O.

612 **FIGURE 6.** Occurrences of metal alloys in chromitites. a, b, c) BSE images of FeNi alloy
613 in chromite and olivine. d) FeCr alloy in chromite. d) EDX spectrum of the FeCr alloy with
614 very minor Mn. Mineral abbreviation: Srp, serpentine.

615 **FIGURE 7.** Inclusions of asphaltum and hexagonal boron nitride (h-BN) in a chromite
616 crystal from sample YK15B. a, b) BSE images and Raman spectra of asphaltum and h-BN.

617 **FIGURE Al.** Backscattered electron image and X-ray maps of Fe, O, Si, Mg and Cr of
618 native Fe. Central part of the native Fe is pure Fe, but its margin partially contains minor Si.
619 Small circles in the native Fe show same position in each map.

620

621 **APPENDIX**

622 Previously separated and identified minerals, native metals and alloys from large samples
623 (500 to > 2000 kg) of the Luobusa podiform chromitite and it wall rock harzburgite (Bai et al.
624 1993, 2000, 2003; Robinson et al. 2004; Xu et al. 2009, 2015; Yang et al. 2014) are
625 summarized in Table A1.

626 The native Fe is near pure iron indicated by EDX spectrum and X-ray element maps that
627 are shown Fig. Al.

This is a preprint, the final version is subject to change, of the American Mineralogist (MSA)
Cite as Authors (Year) Title. American Mineralogist, in press.
(DOI will not work until issue is live.) DOI: http://dx.doi.org/10.2138/am-2016-5436

Table 1 Electron microprobe analyses of FeNi alloys*

Sample	YK15	YK51	YX15	YX15	YX15	YX15	YX 22
Note	in/Ol	in/Ol	in/Chr	in/Chr	in/Chr	in/Chr	in/Chr
Cr	0.9	0.5	1.7	1.9	0.5	0.6	2.9
Fe	13.9	7.0	20.1	15.3	14.2	14.9	20.9
Ni	85.3	92.4	78.1	82.8	85.2	84.4	76.2
Fe/(Fe+Ni)	0.14	0.07	0.21	0.16	0.14	0.15	0.22

* Normalized as element. in/Ol, inclusion in olivine; in/Chr, inclusion in chromite.

This is a preprint, the final version is subject to change, of the American Mineralogist (MSA)
Cite as Authors (Year) Title. American Mineralogist, in press.
(DOI will not work until issue is live.) DOI: http://dx.doi.org/10.2138/am-2016-5436

Table A1 SuR UHP and associated minerals from Luobusa chromitites, Tibet (In previous reports)*

Native elements: C (diamond), Si, Ti, Fe, Cr, Al, Mn
Silicon carbide: moissanite (SiC)
Metal alloys: Ni-Fe-Cr-C, Fe-Ti-Si, Cr-Fe, Ni-Mg-Co, W-Ta and Ni-Mn-Co, Cr-C
PGE and other alloys: Os-Ir, Os-Ir-Ru, Pt-Fe, Ir-Fe and Si-Al
Nitrides: osbornite (TiN) and qinsongite (c-BN)
Oxides: wüstite, Si-rich rutile, type-II TiO_2, coesite, corundum
Fe-silicates with variable amounts of Fe and Si
Crustal xenocrysts: zircon, feldspar, rutile, quartz, kyanite

* Data source: see text. SuR-UHP: super-reducing ultra-high pressure.

This is a preprint, the final version is subject to change, of the American Mineralogist (MSA)
Cite as Authors (Year) Title. American Mineralogist, in press.
(DOI will not work until issue is live.) DOI: http://dx.doi.org/10.2138/am-2016-5436

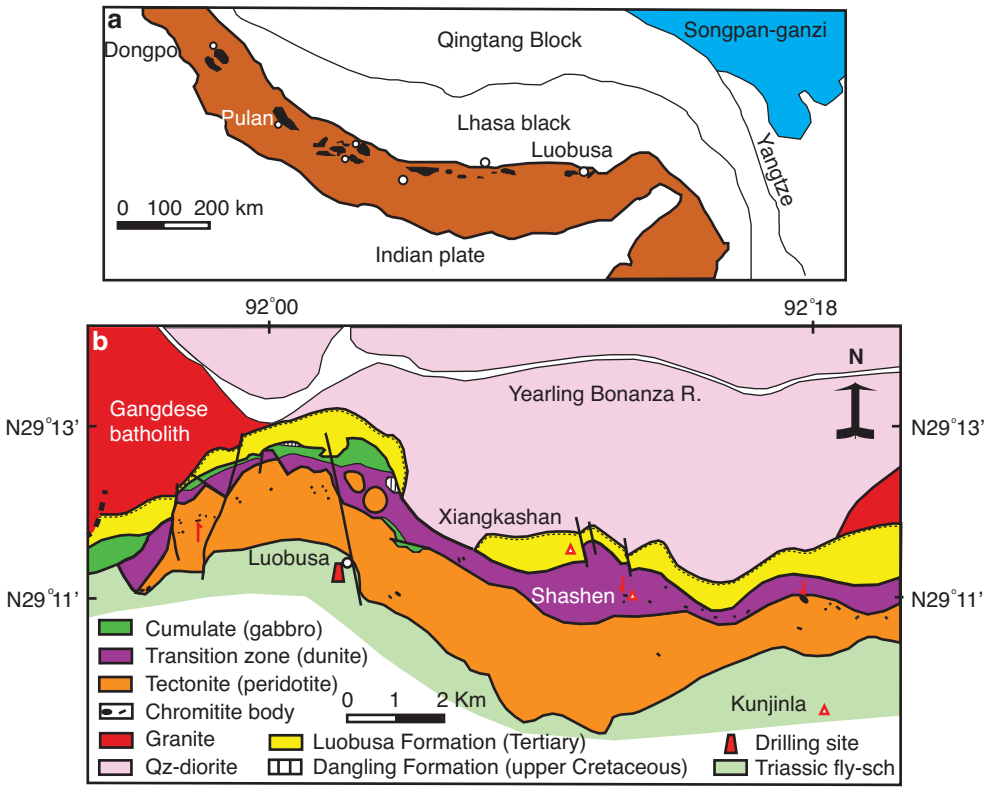

Fig. 1

This is a preprint, the final version is subject to change, of the American Mineralogist (MSA)
Cite as Authors (Year) Title. American Mineralogist, in press.
(DOI will not work until issue is live.) DOI: http://dx.doi.org/10.2138/am-2016-5436

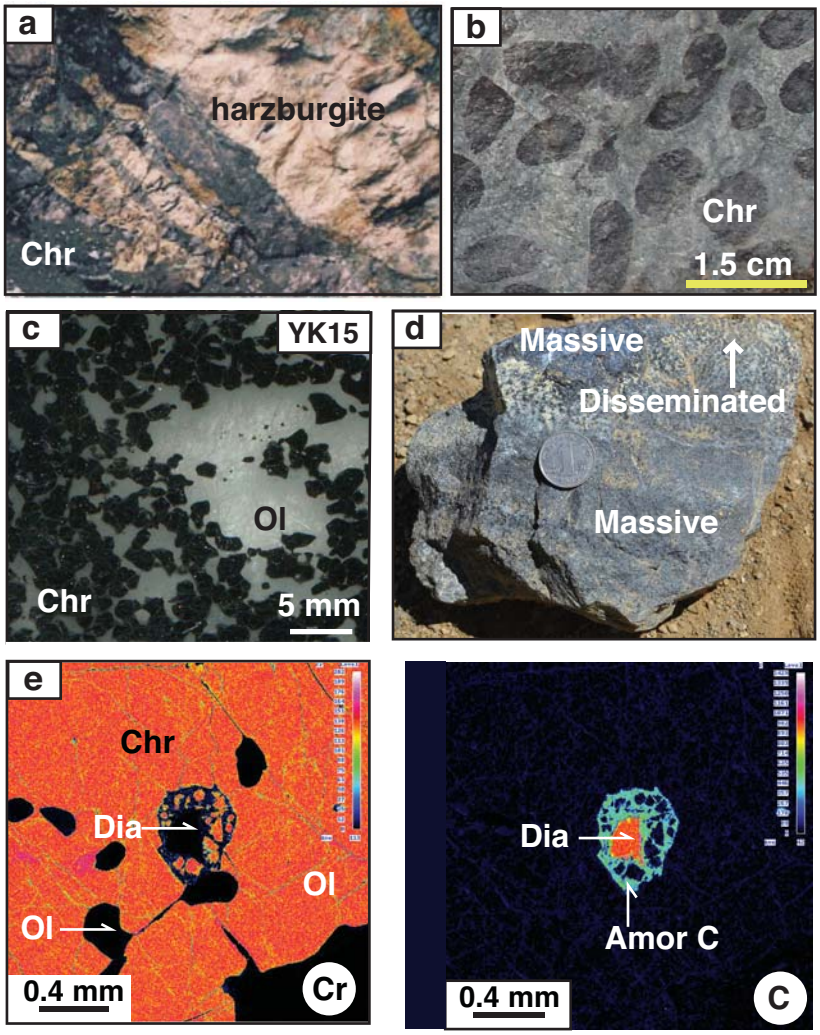

Fig. 2

This is a preprint, the final version is subject to change, of the American Mineralogist (MSA)
Cite as Authors (Year) Title. American Mineralogist, in press.
(DOI will not work until issue is live.) DOI: http://dx.doi.org/10.2138/am-2016-5436

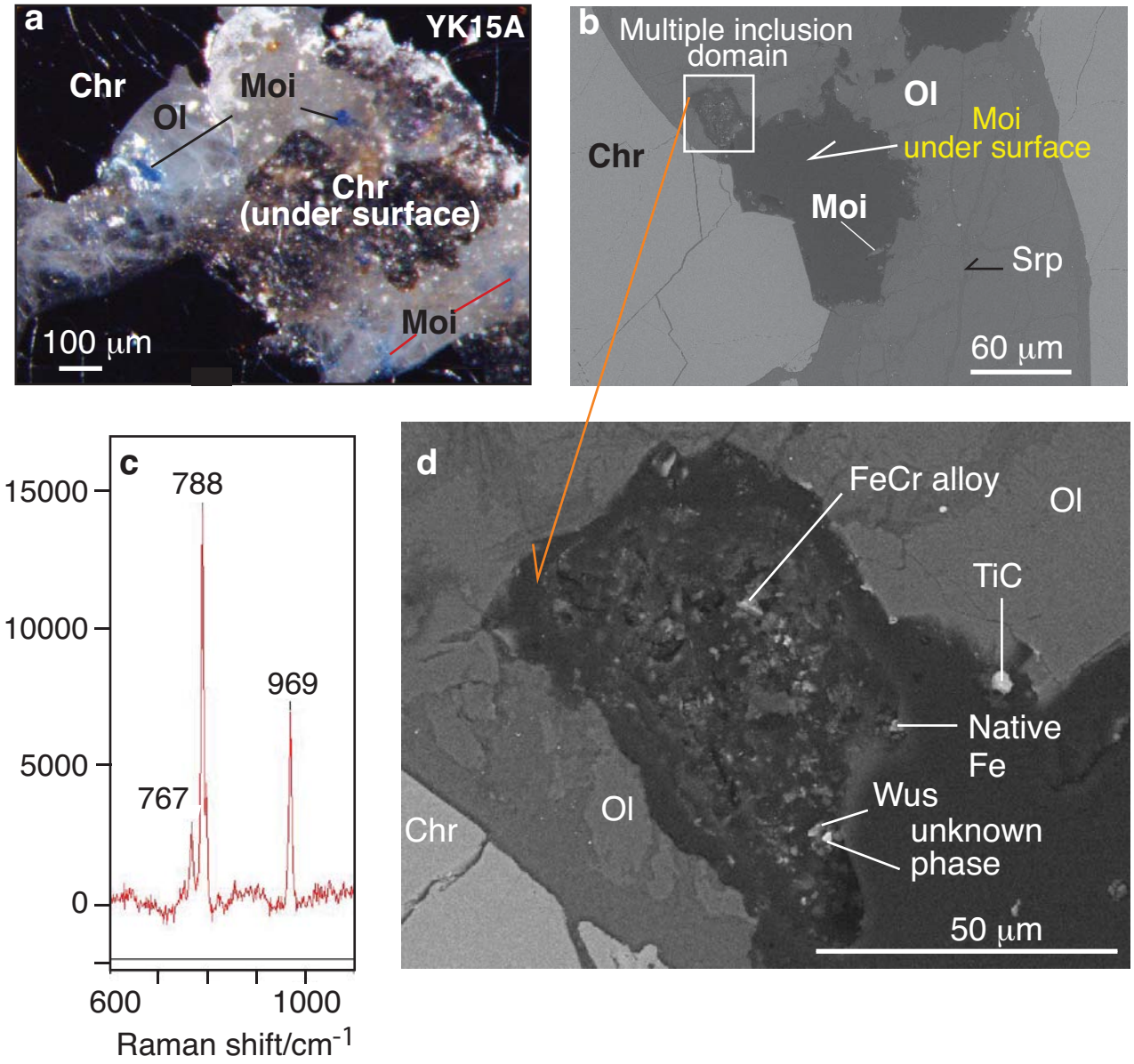

Fig. 3

This is a preprint, the final version is subject to change, of the American Mineralogist (MSA)
Cite as Authors (Year) Title. American Mineralogist, in press.
(DOI will not work until issue is live.) DOI: http://dx.doi.org/10.2138/am-2016-5436

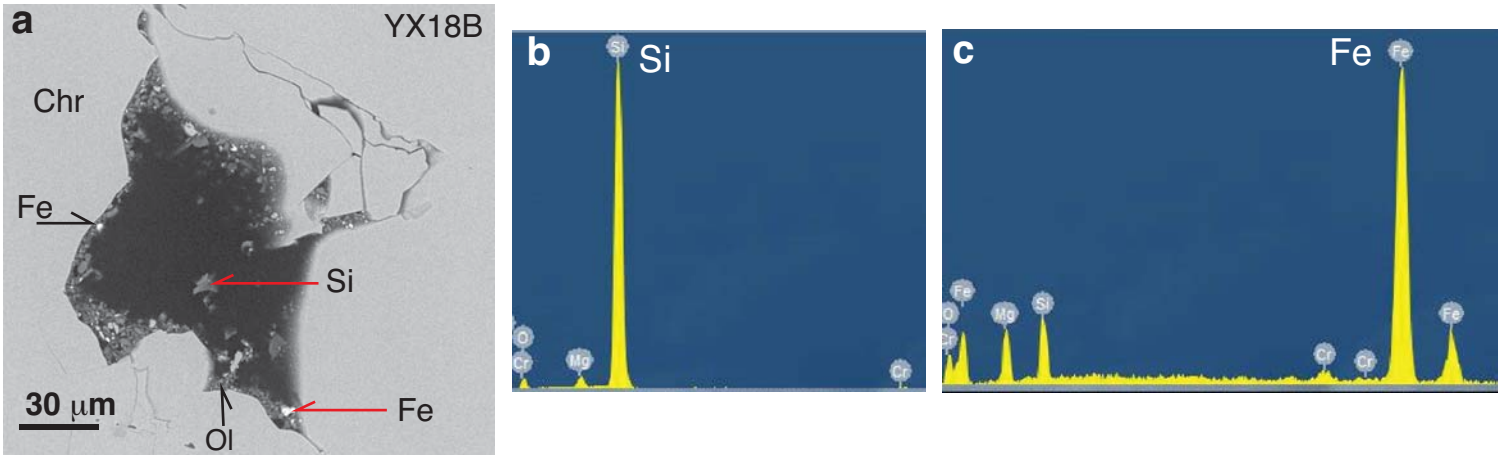

Fig. 4

This is a preprint, the final version is subject to change, of the American Mineralogist (MSA)
Cite as Authors (Year) Title. American Mineralogist, in press.
(DOI will not work until issue is live.) DOI: http://dx.doi.org/10.2138/am-2016-5436

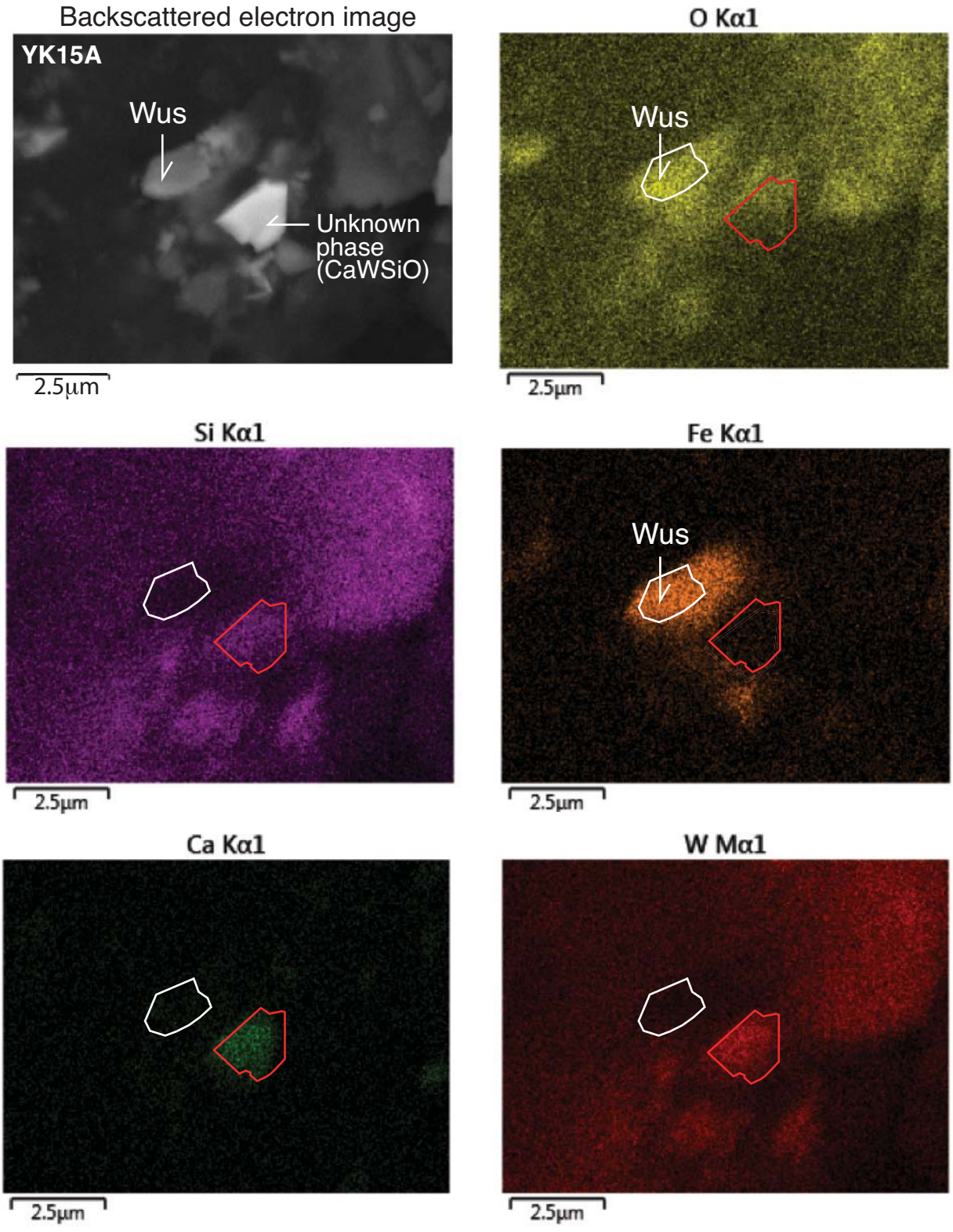

Fig. 5

This is a preprint, the final version is subject to change, of the American Mineralogist (MSA)
Cite as Authors (Year) Title. American Mineralogist, in press.
(DOI will not work until issue is live.) DOI: http://dx.doi.org/10.2138/am-2016-5436

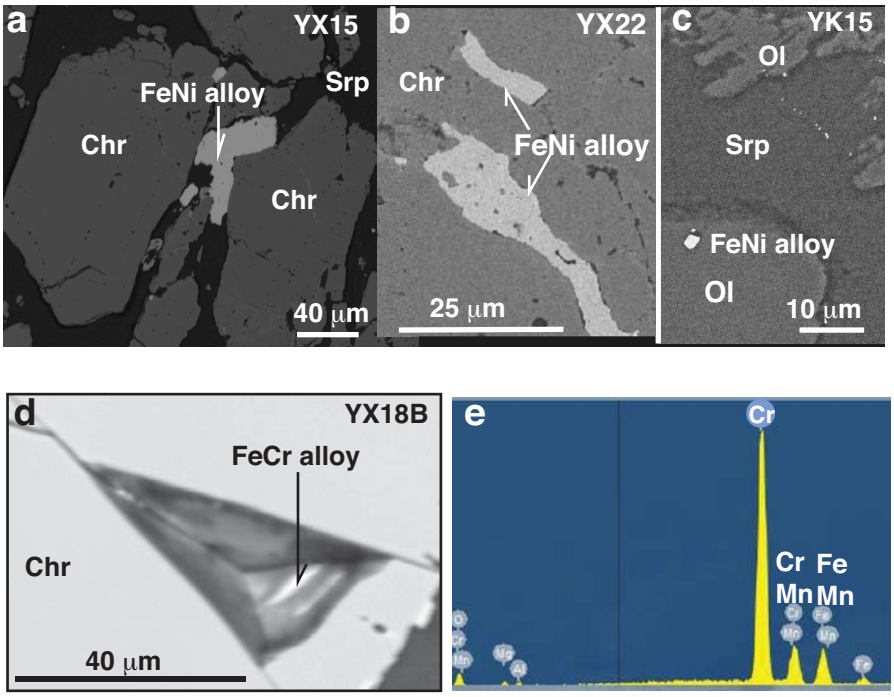

Fig. 6

This is a preprint, the final version is subject to change, of the American Mineralogist (MSA)
Cite as Authors (Year) Title. American Mineralogist, in press.
(DOI will not work until issue is live.) DOI: http://dx.doi.org/10.2138/am-2016-5436

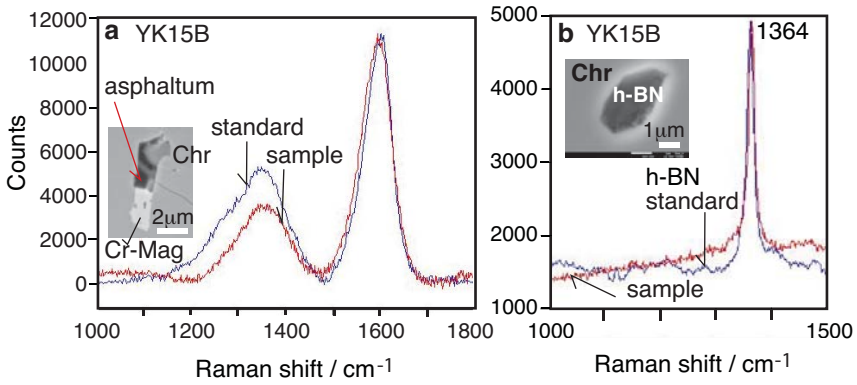

Fig. 7

This is a preprint, the final version is subject to change, of the American Mineralogist (MSA)
Cite as Authors (Year) Title. American Mineralogist, in press.
(DOI will not work until issue is live.) DOI: http://dx.doi.org/10.2138/am-2016-5436

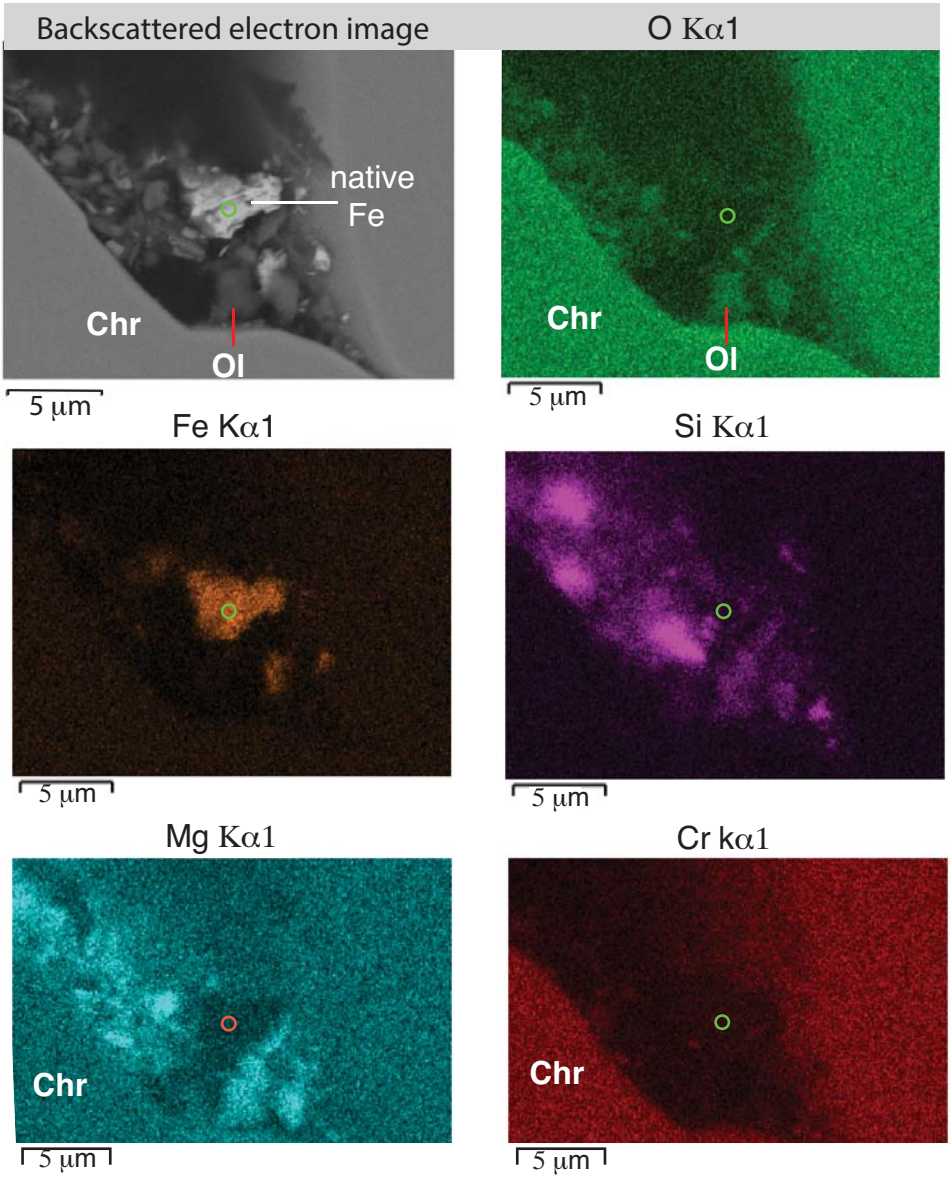

Fig. A1